Effective Debye Lengths in Representative Cislunar Regions

Kaylee Champion[1], and Hanspeter Schaub[2]

***Abstract*—Touchless potential sensing has been investigated in GEO, and as more missions are sent to the cislunar region, this technology may be extended there as well. However, the complexity of the cislunar environment presents novel challenges for touchless potential sensing technology. A chief issue is short Debye lengths, which can be less than 10 meters. Therefore, a model for the electric and potential fields surrounding a charged spacecraft in short Debye regions around the moon is investigated. The vacuum and Debye-Hückel models are presented, and effective Debye lengths are used to expand the models and better represent the environment. The effective Debye length more accurately represents potential shielding and may be up to 6.5 times larger than the electron Debye length in the solar wind dayside region. As a result, touchless potential sensing may be possible at farther, safer distances than expected.**

I. Introduction

Novel active potential sensing of neighboring spacecrafts has been investigated in the Geosynchronous region. This involves a servicing spacecraft directing an electron beam at a target so that secondary electrons [1, 2] and x-rays [3, 4] are emitted from the surface. The incoming signals are then measured, and the servicer utilizes the measurements to infer the potential of the target with respect to its own potential. Knowledge of a target's potential can be used to account for electrostatic perturbations during docking [5, 6] and minimize the risk of discharges during close proximity operations [7]. Awareness of a target's potential is also the first step towards electrostatic actuation, which can be used to detumble or reorbit uncooperative targets, dock incoming bodies, and conduct touchless in-situ servicing [4, 8, 9]. However, cislunar plasma may have Debye lengths less than ten meters, which has not posed an issue in GEO, as the Debye length there is typically up to several hundred meters [10, 11]. The Debye length is a measure of how far a charge's electrostatic effect persists, so short Debye lengths may limit the distance a servicer can sense the potential of a target. Therefore, the effective Debye length in regions around the moon is investigated. The effective Debye length more accurately represents potential and electrostatic shielding in plasma, and it may be several times larger than the Debye length [12].

The cislunar environment is reviewed in Section II. The theory utilized for estimating the potential and electric fields in cold, high density plasma is then presented in Section III. The computational tools used for this research are described in Section IV, and the results and trends are presented in Section V.

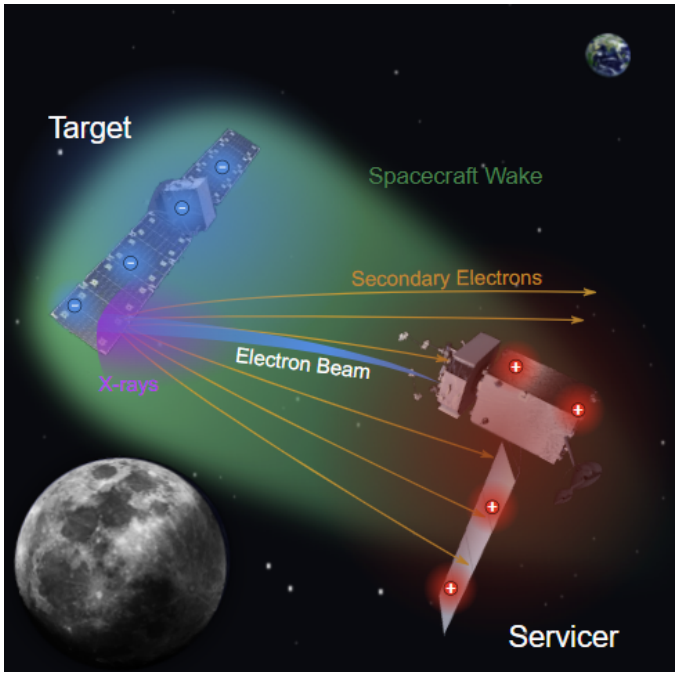

Fig. 1. Touchless potential sensing in cislunar space concept

II. Cislunar Plasma Environment

The cislunar plasma environment can be divided into four regions: solar wind, magnetosheath, magnetotail lobes, and plasma sheet, as shown in Figure 2 [10, 13]. The solar wind region is located outside Earth's magnetic field in the interplanetary magnetic field and flowing solar wind. The magnetotail lobes are located inside the magnetopause and mainly consist of plasma originating from the ionosphere. The plasma sheet is a region of hot plasma located in the center of the magnetotail. It magnetically maps to the auroral oval and splits the magnetotail into its top and bottom lobes. The magnetosheath is the transition region between the magnetotail lobes and the solar wind and mainly consists of solar wind plasma that is deflected around the magnetosphere [14]. Mean, key parameters of these regions are shown in Table I [10].

When the moon is in the solar wind or magnetosheath region, a lunar wake will develop. The moon removes plasma from the environment through processes such as absorption and reflection. If no other processes occurred, this would leave a cylindrical vacuum in the anti-sunward side of the moon.

1: Aerospace Engineering Sciences Department, University of Colorado at Boulder, (email: kach7227@colorado.edu)
2: Aerospace Engineering Sciences Department, University of Colorado at Boulder, (email: Hanspeter.Schaub@colorado.edu)

TABLE I
CISLUNAR REGIONS MEAN PARAMETERS [10]

Region	n_e (m^{-3})	T_e (eV)	v_i ($\frac{m}{s}$)	n_i (m^{-3})	T_i (eV)	λ_D (m)
Magnetotail Lobes	2.0E5	48	170	2.0E5	290	106.7
Plasma Sheet	2.2E5	150	110	2.0E5	780	179.1
Magnetosheath Dayside	9.5E6	18	350	8.0E6	94	9.5
Solar Wind Dayside	6.0E6	11	420	6.0E6	7	6.3

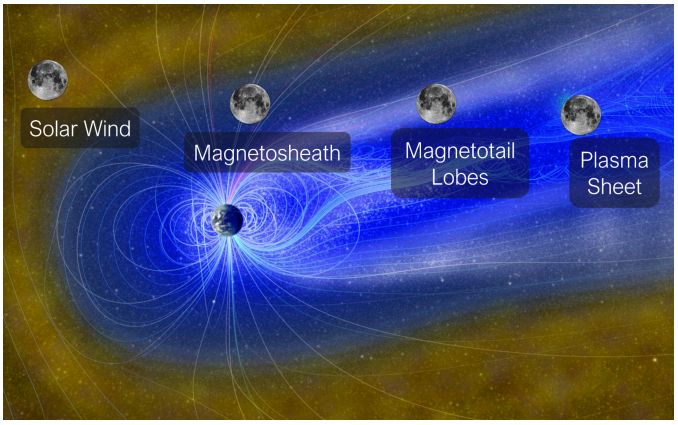

Fig. 2. Cislunar plasma regions defined in the DSNE

However, plasma re-enters through various processes, leaving a low density, complicated plasma structure on the nightside of the moon [15]. As the height above the lunar surface in the wake region increases, the plasma slowly returns to the ambient, undisturbed conditions. More specifically, the density of the plasma increases as the height increases, decreasing the Debye length, as shown in Figure 3 [10].

III. Effective Debye Length Theory

Several analytic approximations of potential and electric fields in plasma have been developed. The appropriate equations depend on several variables, including the properties of the plasma, potential of the spacecraft with respect to the local plasma, and geometry of the spacecraft [16]. Two models are presented in this research: vacuum (Laplace) and Debye-Hückel. Both assume a spherical spacecraft, and their differing approximations provide a range of potential and electric fields that may be present around a charged sphere in plasma [17, 18].

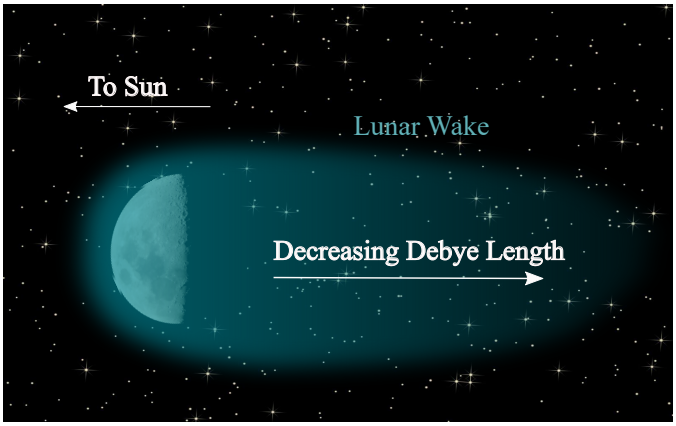

Fig. 3. Lunar wake structure

In a vacuum, the potential field strength at a distance from the center of the sphere is computed as [17]

$$\phi(r) = \frac{V_{SC}R_{SC}}{r}. \tag{1}$$

Where V_{SC} is the potential of the surface, R_{SC} is the radius of the sphere, and r is the distance from the center. This equation is only valid for $r > R_{SC}$. The electric field is the negative gradient of the potential field

$$E(r) = -\nabla_r \phi(r) = \frac{V_{SC}R_{SC}}{r^2}. \tag{2}$$

In a plasma, the potential field is shielded, or drops off more rapidly than in a vacuum. For a sphere with a low surface potential compared to the plasma thermal energy ($eV_{SC} \ll k_B T_e$) the Debye Hückel approximation of the potential field is [17]

$$\phi(r) = \frac{V_{SC}R_{SC}}{r} e^{\frac{-(r-R_{SC})}{\lambda_D}}. \tag{3}$$

Where λ_D is the electron Debye length

$$\lambda_D = \sqrt{\frac{\epsilon_0 k_B T_e}{n_e q_e^2}}. \tag{4}$$

Where ϵ_0 is the permittivity of free space, k_B is Boltzmann's constant, T_e is the electron temperature, n_e is the electron density, and q_e is the elementary charge. The electric field is again the negative gradient of the potential field

$$E(r) = -\nabla_r \phi(r) = \frac{V_{SC}R_{SC}}{r^2} e^{\frac{-(r-R_{SC})}{\lambda_D}} \left(1 + \frac{r}{\lambda_D}\right). \tag{5}$$

The potential and electric field for a 1 meter radius sphere charged to 30kV in a plasma with a Debye length of 6.3 meters is shown in Figures 4 and 5. The vacuum potential and electric fields are the maximum magnitudes possible, as no potential shielding is taken into consideration. There is an exception within a few meters of the surface of the spacecraft, where the Debye-Hückel model predicts a higher electric field than the vacuum model. In the example plots, the Debye-Hückel model shows a larger electric field within 3.25 meters of the surface of the spacecraft. Therefore, the electric field may be larger than expected close to the spacecraft's surface.

The Debye-Hückel model typically overestimates the potential shielding in a plasma, and therefore serves as the minimum fields [18]. Thus, the true fields lie somewhere in between the two models. As the distance from the surface of the spacecraft increases the models diverge and uncertainty increases. Furthermore, as the potential of the spacecraft grows with respect to the plasma temperature ($eV_{SC} > k_B T_e$), the potential field will become closer to the vacuum model. However, the location between the two models is unknown. Therefore, developing a more accurate representation of the

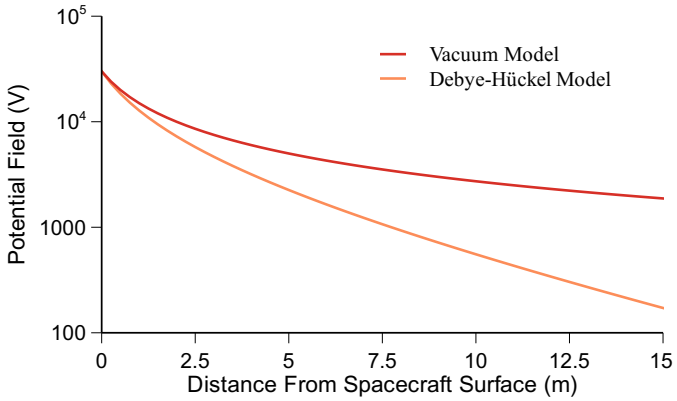

Fig. 4. Potential Field for a 1m Radius Sphere Charged to 30 kV ($\lambda_D = 6.276m$)

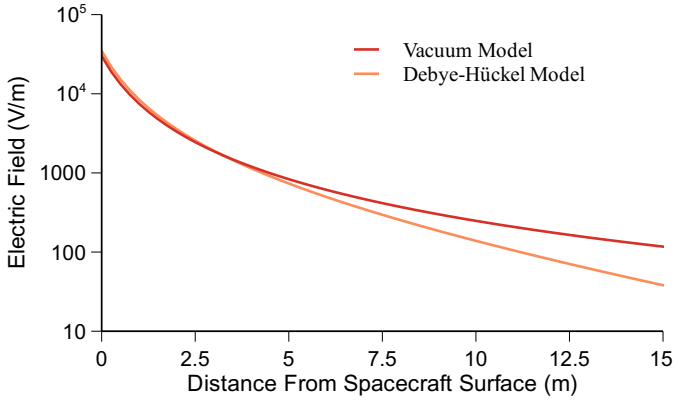

Fig. 5. Electric Field for 1m Radius Sphere Charged to 30 kV ($\lambda_D = 6.276m$)

fields becomes more pressing as the distance from the spacecraft increases and the potential of the surface of the spacecraft increases.

The Debye-Hückel model may be expanded to represent scenario in which $eV_{SC} \ll k_B T_e$. To do so, an effective Debye length is used in place of the electron Debye length [18]. The effective Debye length is simply the Debye length multiplied by a scalar

$$\lambda_{D,eff} = \alpha \lambda_D. \tag{6}$$

$\lambda_{D,eff}$ may then simply be substituted into the Debye-Hückel equations as

$$\phi(r) = \frac{V_{SC} R_{SC}}{r} e^{\frac{-(r-R_{SC})}{\alpha \lambda_D}}, \tag{7}$$

and

$$E(r) = -\nabla_r \phi(r) = \frac{V_{SC} R_{SC}}{r^2} e^{\frac{-(r-R_{SC})}{\alpha \lambda_D}} \left(1 + \frac{r}{\alpha \lambda_D}\right). \tag{8}$$

Finding the effective Debye length is not straightforward. The scalar multiplication term α depends on several variables including the local plasma parameters, spacecraft surface potential, and spacecraft radius [17, 18]. Therefore, computational tools must be utilized.

TABLE II
NASCAP-2K AND SPIS PARAMETERS

Parameter	NASCAP-2k	SPIS
Electron Modeling	Non-linear	PIC
Ion Modeling	Non-linear	PIC
Ion Type	H^+	H^+
Material	Aluminum	Aluminum
Meshing/Grid	0.5 m to 2 m	10 cm to 2 m
External Boundary Size	100 x 100 x 100 m	70 x 70 x 70 m

IV. Computational Tools

Two computational tools are used to calculate the effective Debye length scalar multiplier α: NASCAP-2k and SPIS. NASCAP-2k is a 3D spacecraft charging and plasma interactions code developed as a collaboration between NASA and the Air Force Research Lab [19, 20]. SPIS is a spacecraft plasma interaction software created by the plasma interactions network in Europe (SPINE) [21]. Both programs operate with the same basic principles: the object's geometry and computational space are defined, the plasma properties are inputted, and assumptions/methods of evaluation are selected. However, underlying processes of the programs vary. Therefore, utilizing both tools allows for a better understanding of the range of α terms that may be applicable for a charged spacecraft in a plasma environment and validates the solution. An overview of the parameters defined in NASCAP-2k and SPIS is shown in Table II.

NASCAP-2k defines the computational space using a Cartesian grid. For this problem, three grids are defined with a subdivision ratio of 2 and an outer grid size of 2 meters. Next the interplanetary environment is selected, as this is appropriate for the region [19, 22]. This is chosen out of five options: Geosynchronous, LEO or plume, Auroral, Interplanetary, and Jovian. In each environment, various options are available to calculate potential and electric fields: several analytic options, a hybrid PIC, and a full PIC option. The analytic options are appropriate for simple geometries and compute currents using applied formula. The Hybrid PIC is appropriate for more complex geometries and solves Poisson's equation with space charge given by ion densities from macro-particle tracking and electron densities from analytical formulas [16]. For this problem, the non-linear analytical model was selected, as it is applicable to high and low potentials in a dense plasma. More specifically, the non-linear model solves a convergence formula based on the Langmuir and Blodgett results for current collection by a sphere [16, 23]. The model is also appropriate when the spacecraft velocity and Earth's magnetic field have minimal effect on the charge density within the sheath and is appropriate for low and high spacecraft potentials. The spacecraft will have a velocity with respect to the plasma in the cislunar region and be subject to some magnetic fields, but this first approximation ignores the velocity and magnetic field effects.

SPIS defines the computational space using a mesh, which is built and optimized in GMSH [21]. For this problem, the mesh is given a resolution of 2 meters at the external boundaries and 0.1 meters at the surface of the spacecraft. Once the mesh is built, one of three electric field boundary conditions

must be selected. The Fourier condition is the default and assumes the condition: $E - \alpha V = \beta$, with $\alpha = 1m^{-1}$ and $\beta = 0V/m$ by default. The Dirichlet condition assumes a fixed boundary potential value, and the fixed electric field condition assumes a fixed boundary electric field value. The Dirichlet condition is selected and the boundary potential set to 0V. The external boundary is set significantly far from the surface of the spacecraft as shown in Table II, where 0V may be an accurate assumption. To model the ions and electrons, SPIS offers a Maxwell-Boltzmann and PIC distribution. For this problem, the PIC distribution is selected for both ions and electrons.

Examples of the potential fields calculated in NASCAP-2k and SPIS are shown in Figure 6. Once the potential fields are calculated, the values are exported, and MATLAB's Curvefitter tool is utilized to fit the Debye-Hückel potential field equation to the solution. All variables excluding the α term are inputted as the appropriate constants and the tool then calculated the appropriate α. The data within the first 15 meters of the spacecraft is used, as the potential field near the external boundary is subject to warping.

V. Results

The effective Debye lengths were calculated for the solar wind dayside region, as it has the shortest mean electron Debye length, shown in Table I. Furthermore, the electron temperature is only 11 eV, meaning if the potential of the surface of a spacecraft is only a few volts, the potential of the spacecraft surface is not significantly less than the plasma thermal energy ($eV_{SC} \not\ll k_B T_e$). Figures 7 and 8 show the potential field models for two spherical spacecraft in the solar wind dayside plasma. At 100V, the effective Debye length is already larger than the calculated electron Debye length, and at a higher potential and spacecraft radius the effective Debye length significantly increases. This follows expectations, as the potential field approaches the vacuum model when $eV_{SC} \gg k_B T_e$. The SPIS and NASCAP-2k results show slight differences, but this is expected due to their different potential field calculations. Furthermore, they both display increasing effective Debye length with increasing potential, and the magnitudes of α are comparable.

A. Solar Wind Dayside Trends

The fitting process was performed for spacecrafts with radii ranging from 0.25m to 1m held to potentials from 10V to 10kV. The resulting αs calculated using NASCAP-2k and SPIS are shown in Figures 9 and 10. Both programs show a steep increase in α as the spacecraft potential approaches and begins to exceed the plasma energy (11eV). As the potential continues to increases, α continues to increase, but the rate decreases, resulting in a plateau at high surface potentials. At 10kV, α may be up to six and a half times larger than the electron Debye length. This may allow electrostatic interactions between spacecrafts at farther distances than initially expected.

The NASCAP-2k αs show a strong relationship with the spacecraft radius, as α increases as the radius increases at any given fixed potential. However, SPIS does not show this relationship, as α is approximately the same at all radii. This discrepancy may be the result of insufficient grid or mesh resolution, or errors in fitting. Further investigations are required to rule out these sources of error.

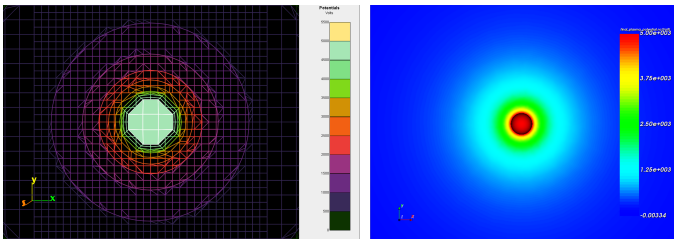

Fig. 6. NASCAP-2k (left) and SPIS (right) Ambient Potentials for 1m Radius Sphere Charged to 5kV

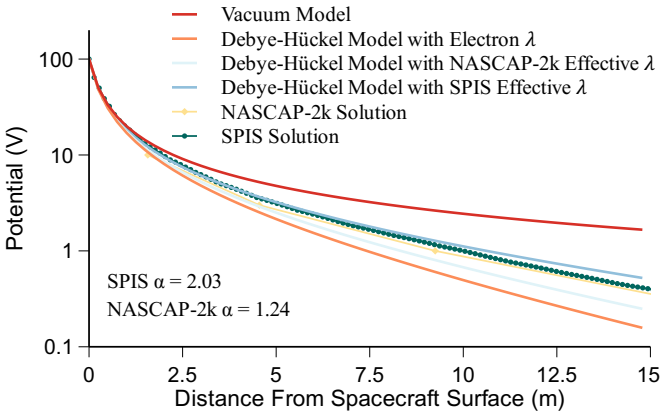

Fig. 7. Potential Field Models for 100V 0.25m Radius Sphere in Mean Solar Wind Dayside Plasma

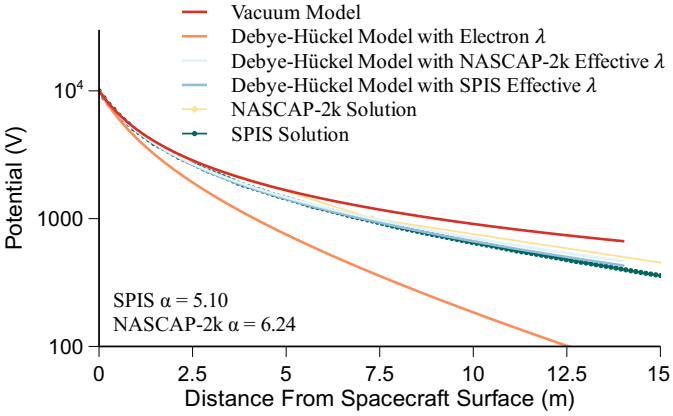

Fig. 8. Potential Field Models for 10kV 1m Radius Sphere in Mean Solar Wind Dayside Plasma

VI. Conclusion

The effective Debye length in the mean solar wind dayside plasma increases with increasing spacecraft potential, reaching up to six and a half times the electron Debye length at 10kV. This is promising, as electrostatic interactions and touchless potential sensing may be possible from farther, safer distances than anticipated. Furthermore, the effective Debye length may

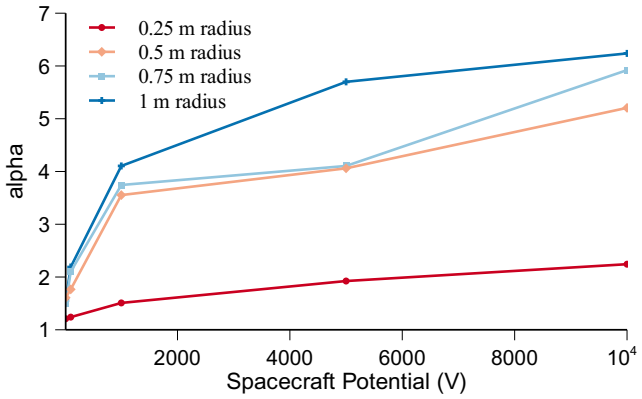

Fig. 9. NASAP-2k α versus Surface Potential

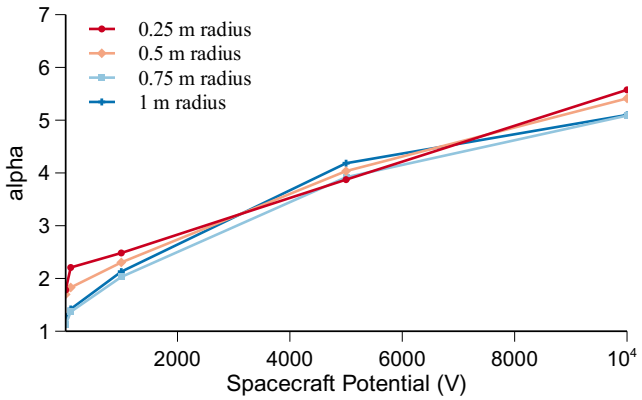

Fig. 10. SPIS α versus Surface Potential

have a dependence on the spacecraft radius. NASCAP-2k shows a distinct increase in α as the spacecraft radius increases, while SPIS does not show the same relationship. The resolution of the grid in NASCAP-2k and mesh in SPIS will be altered to determine if this may be the source of error. This may also provide some added insight into the sensitivity of potential field calculations on computational space resolution.

Future work will involve investigating the effective Debye lengths in the mean magnetosheath dayside region, as the electron Debye length is only 9.5 meters. This work may then be used to approximate electric field strengths around the moon, leading to more accurate investigations of the interactions between a servicer and target. The influence of magnetic fields and spacecraft wakes on the effective Debye lengths is also a subject of future investigation.

Acknowledgements

This work is supported by the National Science Foundation Graduate Research Fellowship Program. The author would like to thank Álvaro Romero-Calvo for his input on the manuscript.

References

[1] M. T. Bengtson, K. T. Wilson, and H. Schaub, "Experimental results of electron method for remote spacecraft charge sensing," *Space Weather*, vol. 18, no. 3, pp. 1–12, 2020.

[2] Álvaro Romero Calvo, J. Hammerl, and H. Schaub, "Touchless potential sensing of complex differentially-charged shapes using secondary electrons," in *AIAA SCITECH 2022 Forum*, 2022.

[3] K. T. H. Wilson and H. Schaub, "X-ray spectroscopy for electrostatic potential and material determination of space objects," *IEEE Transactions on Plasma Science*, vol. 47, no. 8, pp. 3858–3866, Aug. 2019.

[4] K. T. Wilson, M. T. Bengtson, and H. Schaub, "X-ray spectroscopic determination of electrostatic potential and material composition for spacecraft: Experimental results," *Space Weather*, vol. 18, no. 4, p. e2019SW002342, 2020.

[5] K. Wilson and H. Schaub, "Impact of electrostatic perturbations on proximity operations in high earth orbits," *Journal of Spacecraft and Rockets*, vol. 58, no. 5, pp. 1293–1302, 2021.

[6] K. Wilson, A. Romero-Calvo, and H. Schaub, "Constrained guidance for spacecraft proximity operations under electrostatic perturbations," *Journal of Spacecraft and Rockets*, vol. 0, no. 0, pp. 1–13, 2022, *in press*.

[7] H. Schaub, G. G. Parker, and L. B. King, "Challenges and prospects of coulomb spacecraft formation control," *The Journal of the Astronautical Sciences*, vol. 52, no. 1, pp. 169–193, Mar 2004.

[8] F. Casale, H. Schaub, and J. D. Biggs, "Lyapunov optimal touchless electrostatic detumbling of geostationary debris using surface multisphere models," *AIAA Journal of Spacecraft and Rockets*, vol. 58, no. 3, 2021.

[9] H. Schaub and D. F. Moorer, "Geosynchronous large debris reorbiter: Challenges and prospects," *The Journal of the Astronautical Sciences*, vol. 59, no. 1, pp. 161–176, Jun 2012.

[10] F. B. Leahy, "Sls-spec-159, cross-program design specification for natural environments (dsne)," National Aeronautics and Space Administration, Tech. Rep., 2021.

[11] S. Guillemant, V. Génot, J.-C. Matéo-Vélez, R. Ergun, and P. Louarn, "Solar wind plasma interaction with solar probe plus spacecraft," in *Annales Geophysicae*, vol. 30, no. 7. Copernicus GmbH, 2012, pp. 1075–1092.

[12] L. A. Stiles, H. Schaub, K. K. Maute, and D. F. Moorer, "Electrostatically inflated gossamer space structure voltage requirements due to orbital perturbations," *Acta Astronautica*, vol. 84, pp. 109–121, 2013.

[13] J. Halekas, Y. Saito, G. Delory, and W. Farrell, "New views of the lunar plasma environment," *Planetary and Space Science*, vol. 59, no. 14, pp. 1681–1694, 2011.

[14] V. L. Pisacane, *The space environment and its effects on space systems*. American Institute of aeronautics and Astronautics, 2008.

[15] H. Zhang, K. K. Khurana, M. G. Kivelson, V. Angelopoulos, W. X. Wan, L. B. Liu, Q.-G. Zong, Z. Y. Pu, Q. Q. Shi, and W. L. Liu, "Three-dimensional lunar wake reconstructed from artemis data," *Journal of Geophysical Research: Space Physics*, vol. 119, no. 7, pp. 5220–5243, 2014.

[16] V. Davis, M. Mandell, D. Cooke, and D. Ferguson, "Semi-analytic and pic (particle-in-cell) methods for quantifying charging in dense, cold plasma," in *13th Spacecraft Charging Technology Conference, Pasadena, CA*, 2014, pp. 23–27.

[17] C. R. Seubert, L. A. Stiles, and H. Schaub, "Effective coulomb force modeling for spacecraft in earth orbit plasmas," *Advances in Space Research*, vol. 54, no. 2, pp. 209–220, 2014.

[18] N. Murdoch, D. Izzo, C. Bombardelli, I. Carnelli, A. Hilgers, and D. Rodgers, "Electrostatic tractor for near earth object deflection," in *59th International Astronautical Congress*, vol. 29, 2008.

[19] V. Davis, B. Gardner, and M. Mandell, "Nascap-2k version 4.3 users manual," LEIDOS HOLDINGS INC SAN DIEGO CA, Tech. Rep., 2016.

[20] V. Davis and M. Mandell, "Nascap-2k version 4.3 scientific documentation," Leidos, Inc. San Diego United States, Tech. Rep., 2016.

[21] S. Hess, P. Sarrailh, J. Matéo-Vélez, M. Villemant, L. Leclerq, B. Jeanty-Ruard, and A. Trouche, "Spacecraft-plasma interaction software v6," SPINE, Tech. Rep., 2021.

[22] E. M. Willis, H. F. Haviland, J. I. Minow, and V. N. Coffey, "A comparison of artemis data with the lunar plasma design environment for nasa crewed missions," in *Applied Space Environments Conference 2019*, no. M19-7402, 2019.

[23] V. Davis, M. Mandell, B. Gardner, I. Mikellides, L. Neergaard, D. Cooke, and J. Minor, "Validation of nascap-2k spacecraft-environment interactions calculations," in *8th Spacecraft Charging Technology Conference*, 2004.